


### Three-photon electron spin resonances

S. I. Atwood<sup>1</sup>, V. V. Mkhitarian,<sup>2</sup> S. Dhileepkumar<sup>1</sup>, C. Nuibe<sup>1</sup>, S. Hosseinzadeh,<sup>1</sup> H. Malissa<sup>1,2</sup>,  
J. M. Lupton,<sup>1,2</sup> and C. Boehme<sup>1</sup>

<sup>1</sup>*Department of Physics and Astronomy, University of Utah, Salt Lake City, Utah 84112, USA*

<sup>2</sup>*Institut für Experimentelle und Angewandte Physik, Universität Regensburg, 93053 Regensburg, Germany*

 (Received 22 December 2023; revised 19 July 2024; accepted 19 July 2024; published 23 August 2024)

We report the observation of a three-photon resonant transition of charge-carrier spins in an organic light-emitting diode using electrically detected magnetic resonance (EDMR) spectroscopy at room temperature. Under strong magnetic-resonant drive (drive field  $B_1 \sim$  static magnetic field  $B_0$ ), a  $B_0$ -field swept EDMR line emerges when  $B_0$  is approximately three times the one-photon resonance center. Ratios of drive-induced shifts of this line to the shifts of two- and one-photon lines agree with analytical expressions derived from the Floquet Hamiltonian and confirm the nature of these three-photon transitions, enabling access of spin physics to a hitherto inaccessible domain of quantum mechanics.

DOI: [10.1103/PhysRevB.110.L060103](https://doi.org/10.1103/PhysRevB.110.L060103)

The foundational theory of nonperturbative resonant electromagnetic drive regimes for magnetic and electric dipole transitions traces back almost a century to the pioneering contributions of Maria Göppert-Mayer in the 1930s [1]. Her groundbreaking theory on two-photon transitions received some experimental validation from radio frequency and microwave studies starting in the 1950s [2–15] but remained largely unexplored experimentally until the advent of the laser in the 1960s [16–18]. While these breakthroughs catalyzed a revolution in nonlinear optics, profoundly transforming optical spectroscopy and its myriad applications across scientific disciplines [18,19], the experimental investigation of multiphoton *magnetic* dipole transitions has progressed at a notably slower pace compared to their electric dipole counterparts, hindered by formidable technical challenges. In fact, traditional magnetic resonance spectroscopy, requiring tesla-range static magnetic fields, has been largely ineffective in meeting these challenges and has thus not led to significant advancements. It is only with the recent advent of innovative spin-readout mechanisms [20–23]—propelled, for example, by the quest for enhanced magnetometry [24], flexible magnetic resonance imaging [25], and efficient electron spin-based qubits [26]—that new pathways for exploring these phenomena have become available. The resulting interest in harnessing strong-drive-regime magnetic resonance spectroscopy by using spin-dependent electronic transitions in condensed matter systems represents a renewed approach to the study of nonlinear electron spin resonance starting in just the past decade, i.e., since around 2015 [27].

In this Letter, we revisit the question of a spin-resonant three-photon transition and its behavior under strong drive, specifically, its drive-induced resonance shift, which allows for its unambiguous quantitative verification. The significance of this work lies not only in the exploration of three-photon electron spin resonances in a two-level system induced by monochromatic excitation (i.e., irradiation with a rf magnetic field with a single wavelength), of which there are very few reports [20,28,29], but also in their verification through a

Floquet-theory approach that derives analytical expressions for line center shifts and resonance intensities [23]. This not only establishes an experimental niche within the domain of spin/magnetic resonance spectroscopy but, more importantly, also holds profound implications for the broader realm of quantum physics: the emergence of Floquet states under the experimental conditions presented in this Letter potentially offers access to extended spin-coherence time regimes of the employed charge carrier spin states, thereby positioning them as contenders in the quest for robust qubit architectures [22,30–34], including those needed for quantum sensing [35].

Multiphoton magnetic dipole transitions are observed under conditions of nonlinear strong drive, where a linearly polarized driving field  $B_1$  is no longer well approximated by one of its circularly polarized components (rotating wave approximation), i.e., when the ratio of the magnitude of  $B_1$  and the static magnetic field  $B_0$ , which causes the Zeeman splitting, approaches unity [22,23]. Figure 1(a) illustrates an energy-level diagram of an absorptive three-photon transition, which occurs through intermediate *virtual* states (shown as solid gray lines) between two spin eigenstates  $|\downarrow\rangle$  and  $|\uparrow\rangle$ , which are shifted energetically away from the Zeeman separation  $\hbar\gamma B_0$  by the electromagnetic radiation [23], where  $\hbar$  is the reduced Planck constant and  $\gamma$  is the gyromagnetic ratio. Theoretical predictions of the existence and nature of two-level, monochromatic, two-photon magnetic dipole transitions have recently been confirmed through observations of electrically detected magnetic resonance (EDMR) line shifts under strong  $B_1$  from charge-carrier spin pairs in organic bipolar injection devices [23], which can also function as organic light emitting diodes (OLEDs) [36–38]. In this detection scheme, the current through an OLED is measured as  $B_0$  is swept under continuous-wave (cw), radiofrequency (rf) excitation [27]. The current is governed by the recombination rates of weakly magnetic dipole- and exchange-coupled electron-hole polaron pairs (PPs) [39–41]. The recombination rate constants depend on the spin-permutation symmetry (i.e., triplet or singlet state)

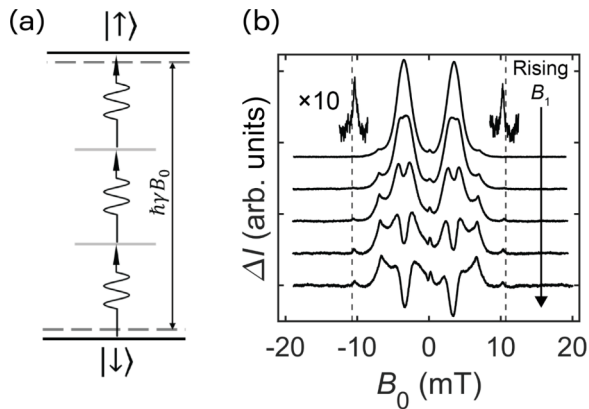


FIG. 1. Electrically detected magnetic resonance (EDMR) spectra of an OLED at high drive-field strengths. (a) Energy-level diagram of a three-photon absorptive transition, which occurs through intermediate virtual states (solid gray lines) between two spin eigenstates  $|\downarrow\rangle$  and  $|\uparrow\rangle$ , which the electromagnetic radiation shifts energetically away from the Zeeman separation  $\hbar\gamma B_0$ . (b) A selection of five single, unaveraged, strong-drive EDMR spectra from an OLED sample with SY-PPV recorded with rf-modulated (20 Hz), lock-in detected cw spectroscopy. The drive field amplitude increases from top to bottom. The magnified three-photon resonances belong to the bottom-most spectrum. The vertical dashed lines indicate an unshifted three-photon resonance. The one-photon resonance bifurcates and inverts due to the ac-Zeeman effect and the spin-Dicke effect [27]. The peak at zero field arises from the quasistatic magnetic-field effect [42].

of the PP, so that changes in the spin permutation symmetry of the ensemble under magnetic resonance conditions lead to detectable changes in the steady-state current of the OLED. Unlike conventional electron paramagnetic resonance spectroscopy, this detection scheme does not require thermal spin polarization and can be conducted at room temperature and with  $B_0$  on the order of millitesla [21–23,27], which is near the order of  $B_1$  that is achievable with conventional copper coils. The lower limit of  $B_0$  is set by the linewidths, which limit the spectroscopic resolution and are primarily governed by hyperfine nuclear spin fields under weak drive and by power broadening under strong drive [21].

Technically, the strong-drive EDMR experiments presented here differ from earlier studies [21–23] significantly because much larger  $B_1$  magnitudes and many more accumulated data sets were needed to observe the much weaker three-photon signatures reliably. We conducted cw EDMR spectroscopy using OLEDs in which the  $\pi$ -conjugated polymer “Super-Yellow” (SY) poly(1,4-phenylene vinylene) (SY-PPV) was used as the active layer. SY-PPV is a commercial organic semiconductor that allowed us to prepare the large number of OLED samples needed to generate a much larger data pool than previous studies that used custom-made deuterated polymer materials [22,23,27]. Figure 1(b) displays five single, unaveraged,  $B_1$ -modulated (20-Hz modulation frequency), lock-in detected SY-PPV EDMR spectra from an OLED sample, recorded within a magnetic field ( $B_0$ ) range of  $\pm 20$  mT, with 100 MHz rf incident drive, for an increasing magnitude of  $B_1$  between  $\sim 1$  and  $\sim 4$  mT. All data discussed in this Letter were recorded at room temperature. The spectra

in Fig. 1(b) verify the strong drive conditions through a variety of qualitative effects that appear with increasing  $B_1$  and that have been discussed in the literature: the inversion of the one-photon peaks due to spin collectivity (the spin-Dicke effect) [27]; the two-photon resonance [22,23]; the Bloch-Siegert shift of the one-photon signal [20,22]; and the non-Bloch-Siegert-type shift of the two-photon resonance [23]. There is also a feature at 0 mT that relates to the so-called quasistatic magnetic field effect and arises due to the dc magnetoresistance induced by  $B_1$  [42]. In addition to all these spectral features, at  $B_0 \approx \pm 10$  mT, the data shown in Fig. 1(b) also reveal a pair of additional resonance peaks that are the focus of the present study. These additional lines cannot be attributed to trivial one-photon transitions caused by amplifier anharmonicities [22,23], as they display a shift toward  $B_0 = 0$  mT with increasing  $B_1$  when compared to the vertical dashed lines, which indicate an unperturbed three-photon resonance at  $3\omega/\gamma = 10.705$  mT, where  $\omega$  is the angular frequency of the driving rf magnetic field. Thus, the quantitative consistency of this shift with predictions from Floquet theory, as discussed in the following, is a crucial prerequisite for the corroboration of this signal as a signature of three-photon electron spin resonance.

For the experiments discussed here, the use of commercially available, fully protonated active OLED layers came at the cost of needing much higher fields  $B_1$  than would be necessary to observe strong-drive phenomena in perdeuterated compounds [22,23]. To generate these fields, the OLEDs were placed inside an rf coil that was part of a resonant rf impedance-matching *tank* circuit developed to maximize the power transfer from the rf amplifier to the coil. The measurements presented in this study were conducted with 100 MHz cw rf drive under square-wave modulation at either 20 Hz, to ensure a fully steady state, or at 1 kHz, yielding comparable EDMR spectra with better signal-to-noise ratio [23]. All data were obtained from a total of 12 SY-PPV OLEDs, each measured separately. The tank circuit was tuned before each measurement series, so that each data set had a different conversion factor between  $B_1$  and the nominal rf amplitude  $A_{rf}$ . The Supplemental Material describes the OLED samples and experimental setup in more detail [43].

Altogether, 1959 EDMR spectra were recorded from all OLED samples. For the analysis of the experimental data, the spectra were subjected to a first-order (linear) baseline correction to account for slow sample drift, and the resonance center fields were determined by averaging the three maxima (or minima for inverted one-photon resonances at higher  $B_1$ ). This method deviates from the procedure reported in Ref. [23], which estimated the line centers by fitting a second-order polynomial to the resonance peaks. In most cases, the two methods yielded the same result, within error, yet the newly introduced method was much faster and no less accurate for the significantly larger data pool. Altogether, 3943 resonance line centers were obtained from one-, two-, and three-photon resonances. The uncertainty in the resonance line centers is dominated by the uncertainty of the  $B_0$  scale, while the uncertainty in the intensity results from the baseline noise. Averages of line centers were made only under identical experimental conditions, i.e., identical  $A_{rf}$  and either ascending or descending  $A_{rf}$ , but not combinations of both, since the conversion

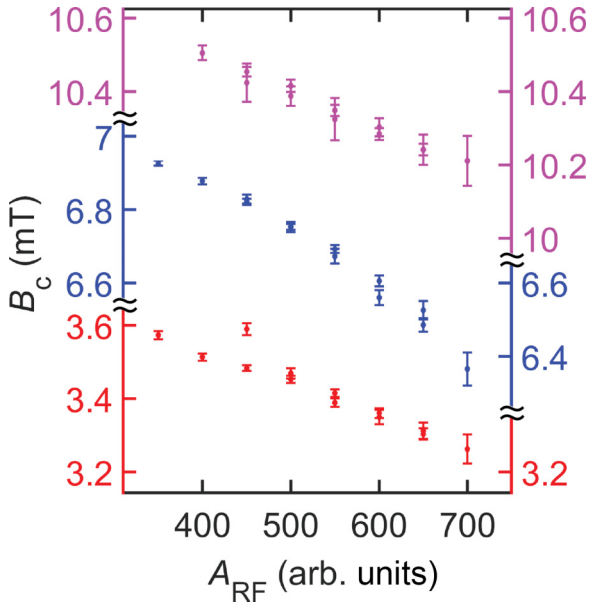


FIG. 2. Averaged resonance line centers  $B_c$  (through identification by the resonance line extrema) from one OLED sample as a function of nominal rf amplitude  $A_{rf}$  (which is nominally proportional to  $B_1$ ) for one-, two-, and three-photon resonances, identified by red, blue, and magenta, respectively. The line centers shown are above the strong-drive limit defined in the text. The right and left vertical scales correspond to identical units yet have different scale breaks to accommodate all data in the same plot. The figure shows two data points for some values of  $A_{rf}$ ; these correspond to data recorded when  $A_{rf}$  was in an ascending or descending sequence. The two points were not averaged because the conversion factor between  $A_{rf}$  and  $B_1$  was observed to change under the effect of strong drive on the coils [43]. The units of  $A_{rf}$  are integers within the digital range (0–2048) controlling the output of the arbitrary wave-form generator in the rf circuit that generated  $B_1$ . The averaged line centers above and below the strong-drive limit for all OLED samples can be found in the Supplemental Material [43].

factor between  $B_1$  and  $A_{rf}$  was observed to change under the effect of strong drive on the coils (see Sec. D of the Supplemental Material [43]). Furthermore, line centers were only averaged by individual OLED samples and not across samples since each experimental run had a different conversion factor between  $B_1$  and  $A_{rf}$ , as explained in the previous paragraph. A weighted average was calculated if all values were within two standard deviations of all the others; otherwise, the mean and standard deviation of the mean ( $\sigma/\sqrt{N}$ ) were calculated.

Figure 2 shows the averaged values of the line centers  $B_c$  for one-, two-, and three-photon resonances as a function of  $A_{rf}$  for spectra obtained from one OLED sample at 20 Hz modulation. The figure shows only those points above the strong-drive limit, which we defined for each individual OLED sample as the points with  $A_{rf}$  higher than the discontinuity in the one-photon resonance shift. The discontinuity has been discussed previously in the context of strong magnetic-resonance drive [23] and is caused by the onset of spin collectivity [22,27], where the one-photon resonance peak inverts and its center is poorly defined. The delineation of the data according to this definition is seen more clearly in the

individual plots of line centers vs  $A_{rf}$  in Fig. S9 of the Supplemental Material [43]. Figures S9–S11 in the Supplemental Material show all averaged line centers above and below the strong-drive limit for all 12 OLED samples [43].

Apart from a single one-photon point at  $A_{rf} = 450$ , the line centers in Fig. 2 decrease monotonically with increasing  $A_{rf}$ , which is nominally proportional to  $B_1$  by a factor that changes when the resonance frequency of the tank circuit changes, e.g., when resistive heating of the rf coil becomes significant (see Sec. D of the Supplemental Material [43]). While this complication prevents a quantitative comparison of the data plotted in Fig. 2 with theoretical predictions, the monotonic relationship between the observed line shifts and  $A_{rf}$  clearly shows that the observed resonance lines cannot be attributed to amplifier harmonics or other artefacts that would display a different shift behavior. Given this effect and the uncertainty of  $B_1$ , a rigorous scrutiny of the shift values obtained requires theoretical predictions that are independent of  $B_1$ . We recently derived such predictions, which require only comparison of one-, two-, and three-photon resonance shifts recorded at the same time, i.e., under identical  $B_1$  conditions [23]. Analytical expressions for  $n$ -photon resonance line centers,  $B_{\gamma_n}$ , are given by

$$B_{\gamma_1} \simeq \frac{\omega}{\gamma} - \frac{\gamma B_1^2 \sin^2 \theta}{16\omega}, \quad n = 1,$$

$$B_{\gamma_n} \simeq n \frac{\omega}{\gamma} - \frac{\gamma B_1^2 \sin^2 \theta}{4\omega} \frac{n}{n^2 - 1}, \quad n > 1, \quad (1)$$

with  $\theta$  the angle between  $\mathbf{B}_1$  and  $\mathbf{B}_0$ , i.e.,  $\theta = 90^\circ$  when the two vectors are perpendicular, as in standard magnetic resonance conditions. Please note that Eq. (1) differs from Eq. (15) in Ref. [23] because  $\theta$  is defined differently here. In Ref. [23],  $\theta$  was defined as the deviation of  $\mathbf{B}_1$  from  $\mathbf{B}_1 \perp \mathbf{B}_0$ . Rearranging these equations and defining the driving-field-induced resonance shift  $\Delta B_{\gamma_n} \equiv n\omega/\gamma - B_{\gamma_n}$ , we find that

$$\frac{\Delta B_{\gamma_n}}{\Delta B_{\gamma_1}} = \frac{4n}{n^2 - 1},$$

$$\frac{\Delta B_{\gamma_n}}{\Delta B_{\gamma_m}} = \frac{n}{m} \frac{m^2 - 1}{n^2 - 1} \quad (2)$$

for any  $n, m > 1$ . The ratio of the two- to one-photon shift from Eq. (2) is  $\Delta B_{\gamma_2}/\Delta B_{\gamma_1} = 8/3 = 2.67$ , which we recently verified experimentally [23]. Since we are testing here for the three-photon resonance, we need to verify the ratios  $\Delta B_{\gamma_3}/\Delta B_{\gamma_2} = 9/16 = 0.5625$  and  $\Delta B_{\gamma_3}/\Delta B_{\gamma_1} = 3/2 = 1.5$ . An experimental confirmation of these ratios only requires accurate estimates of the shifts of two different  $n$ -photon resonances ( $n \geq 1$ ), irrespective of  $B_1$ . Although Eq. (1) cannot be used to estimate the expected shift without knowing  $B_1$ , it can be used to estimate  $B_1$  through the measured shift  $\Delta B_{\gamma_n}$  and the angle  $\theta$ .

Figure 3 shows the drive-induced shifts of the averaged EDMR resonance line centers above the strong-drive limit for (a)  $\Delta B_{\gamma_3}$  vs  $\Delta B_{\gamma_2}$ , (b)  $\Delta B_{\gamma_3}$  vs  $\Delta B_{\gamma_1}$ , and (c)  $\Delta B_{\gamma_2}$  vs  $\Delta B_{\gamma_1}$  obtained for all samples and recorded with  $\mathbf{B}_1 \perp \mathbf{B}_0$ . The solid lines pass through the origin and are set with the slopes predicted by Eq. (2); they are not fits to the data. Each plot shows the same range in abscissa and ordinate to emphasize

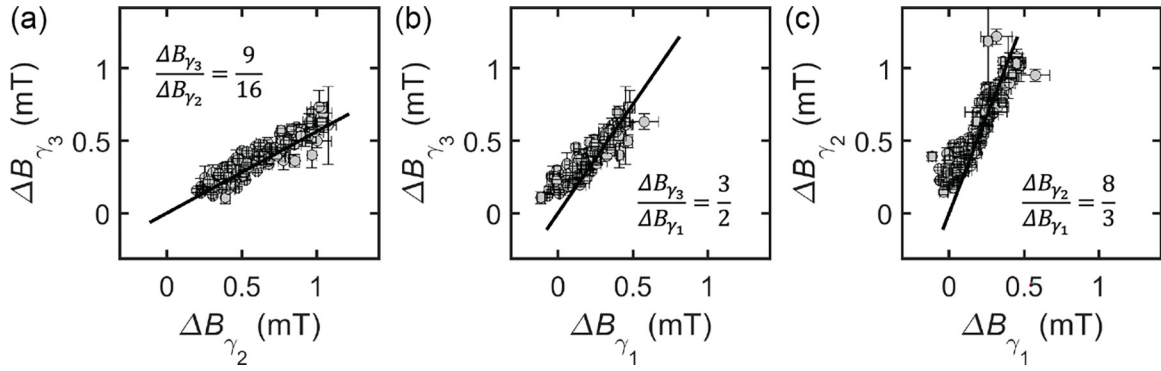


FIG. 3. Drive-induced shifts of averaged resonance line centers of (a) three- vs two-photon, (b) three- vs one-photon, and (c) two- vs one-photon transitions of all measured data sets above the strong-drive limit defined in the text. The solid lines pass through the origin and are set with slopes equal to the ratios stated in the panels; they are not fits to the data. The ratios are predicted by Eq. (2).

the different slopes. Generally, the shift ratios across all OLED samples agree with the predicted ratios. In the data shown in Figs. 3(b) and 3(c), which include the one-photon resonances, the shifts deviate from the predicted slope at lower shift values. This deviation is attributed to the one-photon line centers that are above the strong-drive limit but near the discontinuity from the peak inversion, as discussed above. The Supplemental Material provides a plot of the data in Fig. 3 on normalized scales (Fig. S6) as well as separate plots of the shift ratios obtained from each individual OLED sample (Figs. S12–S14) [43]. As expected, the shift ratios obtained under 1 kHz modulation are the same as those recorded under 20 Hz modulation. Some offsets from the predicted ratios in individual data sets may arise from the fact that the peak extrema are used to approximate the resonance line centers, a reasonable approximation if adjacent broad resonance lines do not overlap.

Following the predictions for multiphoton resonance line shifts under strong drive derived from the Floquet Hamiltonian in Ref. [23], we realize that the effective intensity  $u$  of the three-photon resonance under linearly polarized rf excitation is given by

$$u = \frac{\gamma^3 B_1^3}{32\omega^2} \left| \sin\theta - \frac{9}{8} \sin^3\theta \right|, \quad (3)$$

an expression with a strong dependence of the angle  $\theta$  between  $\mathbf{B}_1$  and  $\mathbf{B}_0$ . This relation has minima at  $\theta = 0^\circ$  and  $70.5^\circ$  and maxima at  $\theta = 33^\circ$  and  $90^\circ$ . While the sample holder was not designed to enable an adjustment of  $\theta$  to arbitrary values, it was possible to change  $\theta$  from  $90^\circ$  to  $69(1)^\circ$  and to conduct measurements on three different OLED samples to ensure reproducibility of the results [43]. Figure 4 shows two single, unaveraged experimental EDMR spectra obtained from the same OLED at the highest  $A_{rf}$ . The black spectrum was recorded first with  $\mathbf{B}_1 \perp \mathbf{B}_0$ , while the gray spectrum was recorded shortly afterward with  $\theta = 69^\circ$ . We note several qualitative differences between the two spectra. The inverted one-photon resonance at  $69^\circ$  is not as strong as its counterpart at  $90^\circ$ , while, conversely, the two-photon line is more intense. These characteristics are qualitatively consistent with the predictions from theory in Ref. [23]. Most significantly, the three-photon resonance is not discernible above the noise level for the nonorthogonal arrangement of  $\mathbf{B}_1$  and  $\mathbf{B}_0$ .

According to Eq. (3), the relative intensity of the three-photon resonance between  $90^\circ$  and  $69^\circ$  is approximately 2.5. We can check these ratios through the statistics of the four spectra measured at  $\theta = 90^\circ$  and the six spectra recorded at  $\theta = 69^\circ$ . The mean three-photon resonance intensity of the four spectra at  $90^\circ$  is  $0.0038 \pm 0.0007$  arbitrary units, while the mean of the baseline noise at  $69^\circ$  is  $0.0009 \pm 0.0003$  arbitrary units. The ratio of the two is therefore  $4 \pm 2$ , which shows that the noise level is not below the theoretically predicted resonance intensity, within the error. Additional spectra, results from numerical simulations, and the values of the averaged line centers as a function of  $A_{rf}$  at  $\theta = 69^\circ$  for each of the three OLEDs utilized, as well as the shift ratios for  $\Delta B_{\gamma_2}$  vs  $\Delta B_{\gamma_1}$ , are given in the Supplemental Material [43]. Note that none of the line centers from the angled data are shown in Fig. 3 because they do not fall within the strong-drive limit defined above.

In conclusion, we find that room temperature, cw, low-field, strong-drive EDMR spectroscopy of charge carrier spin states in the  $\pi$ -conjugated polymer SY-PPV confirms the existence of three-photon magnetic-dipole transitions through the characteristic shifts of the resonance lines with drive strength and magnetic field orientation as predicted by theory [22,23]. The results of this study elucidate the nature of these spin transitions and open up pathways to a variety of

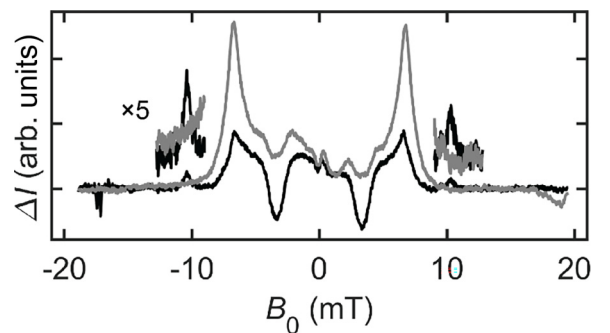


FIG. 4. Single, unaveraged OLED EDMR spectra obtained at the same nominal rf amplitudes  $A_{rf}$  for  $\theta = 69^\circ$  (gray) and  $\theta = 90^\circ$  (black). The data at  $\theta = 69^\circ$  do not show any discernible three-photon resonances.

previously inaccessible spin effects and their potential applications, including the use of three-photon transitions for spin-qubit initialization and manipulation, as well as strong magnetic-drive induced protection of spin coherence [22].

This work was supported by the U.S. Department of Energy, Office of Basic Energy Sciences, Division of Materials

Sciences and Engineering under Award No. DE-SC0000909. H.M. and V.V.M. acknowledge support from the Deutsche Forschungsgemeinschaft (DFG, German Research Foundation) (Project ID No. 314695032–SFB 1277, subproject B03). S.D. and C.N. acknowledge support through the University of Utah’s College of Science Student Research Initiative.

- 
- [1] M. Göppert-Mayer, Über elementarakte mit zwei quantensprüngen, *Ann. Phys.* **401**, 273 (1931).
- [2] V. Hughes and L. Grabner, The radiofrequency spectrum of  $\text{Rb}^{85}\text{F}$  and  $\text{Rb}^{87}\text{F}$  by the electric resonance method, *Phys. Rev.* **79**, 314 (1950).
- [3] L. Grabner and V. Hughes, Further evidence for a two quantum transition in molecular spectroscopy, *Phys. Rev.* **82**, 561 (1951).
- [4] J. Brossel, B. Cagnac, and A. Kastler, Observations de résonances magnétiques à plusieurs quanta sur un jet d’atomes de sodium orientés optiquement, *C. R. Acad. Sci.* **237**, 984 (1953).
- [5] J. Brossel, B. Cagnac, and A. Kastler, Résonance magnétique sur des atomes orientés optiquement, *J. Phys. Radium* **15**, 6 (1954).
- [6] P. Kusch, Some observations of double- and triple-quantum transitions, *Phys. Rev.* **93**, 1022 (1954).
- [7] R. Braunstein and J. W. Trischka, Molecular constants and nuclear-molecular interactions of  $\text{Li}^{7}\text{F}^{19}$  by the molecular beam electric resonance method, *Phys. Rev.* **98**, 1092 (1955).
- [8] V. W. Hughes and J. S. Geiger, Two-quantum transitions in the microwave Zeeman spectrum of atomic oxygen, *Phys. Rev.* **99**, 1842 (1955).
- [9] J. Margerie and J. Brossel, Transitions à plusieurs quanta électromagnétiques, *C. R. Acad. Sci.* **241**, 373 (1955).
- [10] J. Brossel, J. Margerie, and J. Winter, Effet Bloch-Siegert dans les résonances à plusieurs quanta, *C. R. Acad. Sci.* **241**, 556 (1955).
- [11] W. Anderson, Nuclear resonance saturation effects and multiple-quantum transitions, *Phys. Rev.* **104**, 850 (1956).
- [12] J. I. Kaplan and S. Meiboom, Double-quantum transitions in nuclear magnetic resonance spectra of liquids, *Phys. Rev.* **106**, 499 (1957).
- [13] P. P. Sorokin, I. L. Gelles, and W. V. Smith, Multiple quantum transitions in paramagnetic resonance, *Phys. Rev.* **112**, 1513 (1958).
- [14] J. W. Orton, P. Auzins, and J. E. Wertz, Double-quantum electron spin resonance transitions of nickel in magnesium oxide, *Phys. Rev. Lett.* **4**, 128 (1960).
- [15] J. Burget, M. Odehnal, V. Petříček, J. Šácha, and L. Trlifaj, Double quantum transitions in free radicals, *Czech. J. Phys. B* **11**, 719 (1961).
- [16] T. H. Maiman, Stimulated optical radiation in ruby, *Nature (London)* **187**, 493 (1960).
- [17] W. Kaiser and C. G. B. Garrett, Two-photon excitation in  $\text{CaF}_2:\text{Eu}^{2+}$ , *Phys. Rev. Lett.* **7**, 229 (1961).
- [18] H. Mahr, Two-photon absorption spectroscopy, in *Quantum Electronics: A Treatise*, edited by H. Rabin and C. L. Tang (Academic Press, New York, 1975).
- [19] V. Nathan, A. H. Guenther, and S. S. Mitra, Review of multiphoton absorption in crystalline solids, *J. Opt. Soc. Am. B* **2**, 294 (1985).
- [20] J. P. Ashton and P. M. Lenahan, Multiple-photon transitions in electrically detected magnetic resonance measurements of  $4\text{H-SiC}$  transistors, *Phys. Rev. B* **102**, 020101(R) (2020).
- [21] S. Jamali, G. Joshi, H. Malissa, J. M. Lupton, and C. Boehme, Monolithic OLED-microwire devices for ultrastrong magnetic resonant excitation, *Nano Lett.* **17**, 4648 (2017).
- [22] S. Jamali, V. V. Mkhitarian, H. Malissa, A. Nahlawi, H. Popli, T. Grünbaum, S. Bange, S. Milster, D. M. Stoltzfus, A. E. Leung *et al.*, Floquet spin states in OLEDs, *Nat. Commun.* **12**, 465 (2021).
- [23] S. I. Atwood, S. Hosseinzadeh, V. V. Mkhitarian, T. H. Tennaheva, H. Malissa, W. Jiang, T. A. Darwish, P. L. Burn, J. M. Lupton, and C. Boehme, Non-Bloch-Siegert-type power-induced shift of two-photon electron paramagnetic resonances of charge-carrier spin states in an OLED, [arXiv:2310.14180](https://arxiv.org/abs/2310.14180).
- [24] W. J. Baker, K. Ambal, D. P. Waters, R. Baarda, H. Morishita, K. van Schooten, D. R. McCamey, J. M. Lupton, and C. Boehme, Robust absolute magnetometry with organic thin-film devices, *Nat. Commun.* **3**, 898 (2012).
- [25] V. Han and C. Liu, Multiphoton magnetic resonance in imaging: A classical description and implementation, *Magn. Reson. Med.* **84**, 1184 (2020).
- [26] S. Bertaina, L. Chen, N. Groll, J. Van Tol, N. S. Dalal, and I. Chiorescu, Multiphoton coherent manipulation in large-spin qubits, *Phys. Rev. Lett.* **102**, 050501 (2009).
- [27] D. P. Waters, G. Joshi, M. Kavand, M. E. Limes, H. Malissa, P. L. Burn, J. M. Lupton, and C. Boehme, The spin-Dicke effect in OLED magnetoresistance, *Nat. Phys.* **11**, 910 (2015).
- [28] B. Clerjaud and A. Gelineau, Observation of electron paramagnetic resonances at multiples of the “classical” resonance magnetic field, *Phys. Rev. Lett.* **48**, 40 (1982).
- [29] V. Morozov, O. Antzutkin, A. Koptuyug, and A. B. Doktorov, Multiquantum resonances in low-field optically detected ESR of radical-ion pairs, *Mol. Phys.* **73**, 517 (1991).
- [30] H. Hatanaka and N. Tabuchi, New line-narrowing effect in triple-quantum resonance in a two-level NMR system, *J. Magn. Reson.* **155**, 119 (2002).
- [31] A. Laucht, R. Kalra, S. Simmons, J. P. Dehollain, J. T. Muhonen, F. A. Mohiyaddin, S. Freer, F. E. Hudson, K. M. Itoh, D. N. Jamieson *et al.*, A dressed spin qubit in silicon, *Nat. Nanotechnol.* **12**, 61 (2017).
- [32] H. Morishita, T. Tashima, D. Mima, H. Kato, T. Makino, S. Yamasaki, M. Fujiwara, and N. Mizuochi, Extension of the coherence time by generating MW dressed states in a single NV centre in diamond, *Sci. Rep.* **9**, 13318 (2019).
- [33] K. C. Miao, J. P. Blanton, C. P. Anderson, A. Bourassa, A. L. Crook, G. Wolfowicz, H. Abe, T. Ohshima, and D. D. Awschalom, Universal coherence protection in a solid-state spin qubit, *Science* **369**, 1493 (2020).

- [34] H. Tabuchi, Y. Matsuzaki, N. Furuya, Y. Nakano, H. Watanabe, N. Tokuda, N. Mizuochi, and J. Ishi-Hayase, Temperature sensing with RF-dressed states of nitrogen-vacancy centers in diamond, *J. Appl. Phys.* **133**, 024401 (2023).
- [35] C. L. Degen, F. Reinhard, and P. Cappellaro, Quantum sensing, *Rev. Mod. Phys.* **89**, 035002 (2017).
- [36] R. Miller, K. J. van Schooten, H. Malissa, G. Joshi, S. Jamali, J. M. Lupton, and C. Boehme, Morphology effects on spin-dependent transport and recombination in polyfluorene thin films, *Phys. Rev. B* **94**, 214202 (2016).
- [37] T. H. Tannahewa, S. Hosseinzadeh, S. I. Atwood, H. Popli, H. Malissa, J. M. Lupton, and C. Boehme, Coherent and incoherent spin-relaxation dynamics of electron-hole pairs in a  $\pi$ -conjugated polymer at low magnetic fields, *Phys. Rev. B* **109**, 075303 (2024).
- [38] D. R. McCamey, K. J. van Schooten, W. J. Baker, S.-Y. Lee, S.-Y. Paik, J. M. Lupton, and C. Boehme, Hyperfine-field-mediated spin beating in electrostatically bound charge carrier pairs, *Phys. Rev. Lett.* **104**, 017601 (2010).
- [39] F. A. Castro, G. B. Silva, L. F. Santos, R. M. Faria, F. Nüesch, L. Zuppiroli, and C. F. O. Graeff, Electrically detected magnetic resonance of organic and polymeric light emitting diodes, *J. Non-Cryst. Solids* **338–340**, 622 (2004).
- [40] D. R. McCamey, H. A. Seipel, S.-Y. Paik, M. J. Walter, N. J. Borys, J. M. Lupton, and C. Boehme, Spin Rabi flopping in the photocurrent of a polymer light-emitting diode, *Nat. Mater.* **7**, 723 (2008).
- [41] W. J. Baker, D. R. McCamey, K. J. van Schooten, J. M. Lupton, and C. Boehme, Differentiation between polaron-pair and triplet-exciton Polaron spin-dependent mechanisms in organic light-emitting diodes by coherent spin beating, *Phys. Rev. B* **84**, 165205 (2011).
- [42] S. Milster, T. Grünbaum, S. Bange, S. Kurrmann, H. Kraus, D. M. Stoltzfus, A. E. Leung, T. A. Darwish, P. L. Burn, C. Boehme *et al.*, Perdeuterated conjugated polymers for ultralow-frequency magnetic resonance of OLEDs, *Angew. Chem. Int. Ed.* **59**, 9388 (2020).
- [43] See Supplemental Material at <http://link.aps.org/supplemental/10.1103/PhysRevB.110.L060103> for details on the OLED samples and experimental setup and for supporting data, which includes Refs. [44–46].
- [44] M. Kavand, D. Baird, K. van Schooten, H. Malissa, J. M. Lupton, and C. Boehme, Discrimination between spin-dependent charge transport and spin-dependent recombination in  $\pi$ -conjugated polymers by correlated current and electroluminescence-detected magnetic resonance, *Phys. Rev. B* **94**, 075209 (2016).
- [45] H. Malissa, M. Kavand, D. P. Waters, K. J. van Schooten, P. L. Burn, Z. V. Vardeny, B. Saam, J. M. Lupton, and C. Boehme, Room-temperature coupling between electrical current and nuclear spins in OLEDs, *Science* **345**, 1487 (2014).
- [46] J. Mispelter, M. Lupu, and A. Briguet, *NMR Probeheads for Biophysical and Biomedical Experiments* (Imperial College Press, London, 2015), pp. 197–267.